Proceedings Paper:
Taras, P., Li, G. orcid.org/0000-0002-5956-4033, Zhu, Z.Q. et al. (2 more authors) (2019) Comparative investigation of stator-mounted permanent magnet machines under fault conditions. In: The Journal of Engineering. The 9th International Conference on Power Electronics, Machines and Drives (PEMD 2018), 17-19 Apr 2018, Liverpool, UK. IET , pp. 4241-4246.

https://doi.org/10.1049/joe.2018.8203

The Journal of Engineering

The 9th International Conference on Power Electronics, Machines and Drives (PEMD 2018)

IET Journals
The Institution of Engineering and Technology

Comparative investigation of stator-mounted permanent magnet machines under fault conditions

eISSN 2051-3305
Received on 25th June 2018
Accepted on 30th July 2018
E-First on 9th May 2019
doi: 10.1049/joe.2018.8203
www.ietdl.org

Petrica Taras[1] ✉, Guang-Jin Li[1], Zi-Qiang Zhu[1], Martin P. Foster[1], David A. Stone[1]

[1]*The University of Sheffield, UK*

✉ *E-mail: petrica.taras@sheffield.ac.uk*

Abstract: Here, machines having permanent magnets (PM) mounted in the stator are compared during fault operations such as armature winding short circuits. The magnet potential irreversible demagnetisation is also investigated due to the fact that the PMs are placed close to the armature coils (heat sources) and hence are prone to temperature-related demagnetisations. It is found that the doubly salient and flux reversal machines have inherently higher fault tolerant capabilities when compared with the switched-flux one. To the point of view of demagnetisation withstand capability, the doubly salient topology stands out as the most robust one while the switched flux is the weakest one.

1 Introduction

The topologies considered here, as shown in Fig. 1, are the switched-flux permanent magnet (PM) machine (SFPMM) [1], doubly salient PM machine (DSPMM) [2], and flux reversal PM machine (FRPMM) [3]. Both windings and PMs are located in the stator and, therefore, are stationary. The rotor is a salient piece of iron, making the entire structure very robust at high speeds. Potential applications of these topologies are in the automotive and aircraft industries.

It has been established in literature [4–6] that compared to the SFPMM, the DSPMM and the FRPMM have performance limitations due to the location of PMs and their magnetisation directions. For the DSPMM, its flux linkage is unipolar, and hence reducing the induced back-EMF. For the FRPMM, having the PM located in the air gap is problematic, which exposes them to the demagnetisation issues due to generally small PM thickness. The SFPMM, on the other hand, has been favourably compared with established topologies like the surface-mounted and interior PM machines [5, 7].

However, having the PMs located closer to the windings (heat sources) in the stator-mounted PM machines raises the issue of potential magnet irreversible demagnetisation [8–10]. This can be even more serious under fault operation such as inter-turn short-circuit which can lead to significant local temperature increase. However, the fault tolerant capabilities under inter-turn short-circuit fault for the SFPMM, the DSPMM and the FRPMM have not been compared in literature. To fill in this gap, a comparison from the point of view of irreversible demagnetisation is essential for all three considered topologies and will be carried out here.

2 Model description

The specifications of the investigated machines are given in Table 1. In order to make a fair and simple comparison, the outer diameter and active length, the winding cross-section area and the rated current are the same for all machine topologies. This in turn ensures that the copper losses, an important source of heat, are kept the same. In addition, for all topologies, the windings are double layer type. However, the split ratio and PM volume have been optimised to achieve the highest possible output torque for each machine topology. It is found that the SFPMM can produce much higher torque than the other two machines with the DSPMM being the lowest one. However, the DSPMM and the FRPMM require a much smaller PM volume than SFPMM (see Table 1), making them more attractive from the cost point of view. The PM grade, for all topologies, is N35H [11].

Here, there will be three stages in the investigations:

i. 2D FE models parameters extraction;
ii. Matlab/Simulink models of healthy and faulty operations;
iii. 2D FE models using an accurate PM model (but also more time consuming to solve) to assess demagnetisation occurrence.

First, the 2D FE models of the aforementioned machine topologies are developed to extract characteristics such as the cogging torque, the self- and mutual-inductances and the back-EMF which are both rotor position and temperature-dependent. The thermal characteristics are obtained by considering the PM material working at the assumed temperatures.

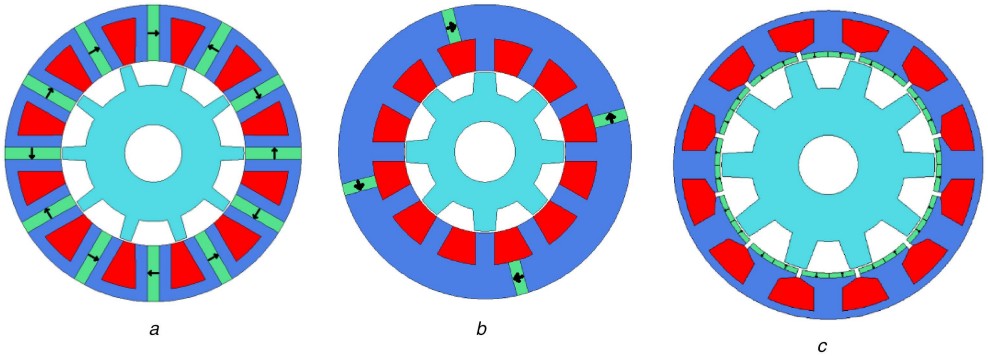

Fig. 1 *Cross-sections of stator mounted PM machines investigated here*
(a) SFPMM, ***(b)*** DSPMM, ***(c)*** FRPMM

Table 1 Specification of investigated machines (SFPMM/DSPMM/FRPMM)

stator slot number	12	RMS rated armature current, A	11
rotor pole number	10/8/10	Average torque, Nm	2.2/1.0/1.5
stator outer radius, mm	45	PM volume, mm^3	18360/3750/ 5460
split ratio	0.62/0.55/ 0.70	PM thickness, mm	3.6/3.6/1.2

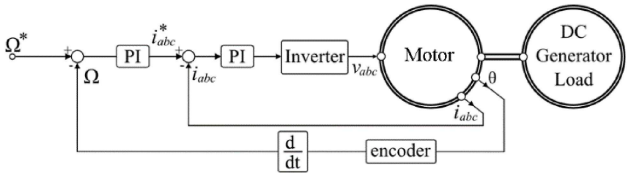

Fig. 2 *Simplified diagram of the Matlab/Simulink model*

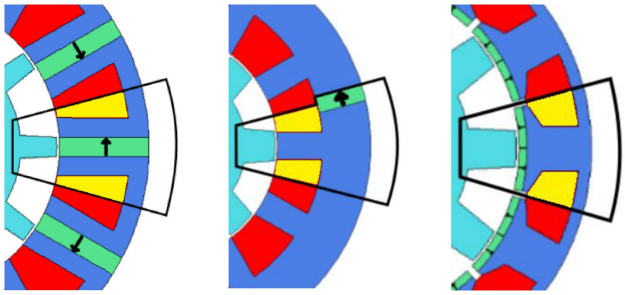

Fig. 3 *Inter-turn short-circuit coil and PM locations*

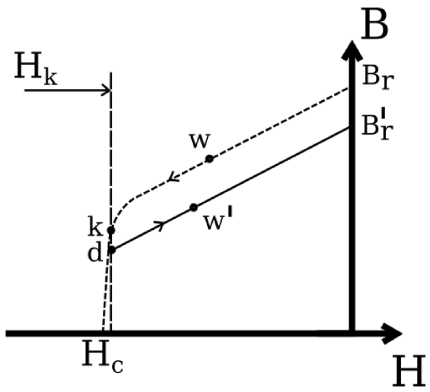

Fig. 4 *PM model used to assess the irreversible demagnetisation*

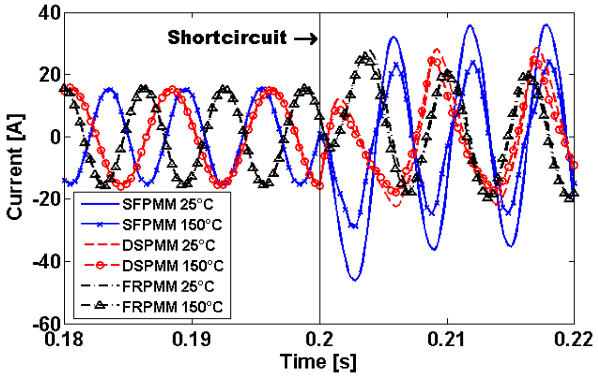

Fig. 5 *Short-circuit current comparison for all topologies during fault conditions at 1000 rpm, low (25°C) and high (150°C) temperatures*

Second, these results are stored in look-up tables and used in the Matlab/Simulink models that implement the voltage and torque equations [12–15]. The machine voltage equations used in the Simulink/Matab models are as follows:

$$[v] = [R] \times [i] + \frac{\mathrm{d}([L] \times [i])}{\mathrm{d}t} + [e] \tag{1}$$

where $[v]$ and $[i]$ are the phase voltages and currents in vector form, $[e]$ is the back-EMF, $[R]$ and $[L]$ are the phase resistance and inductance matrices. The mechanical equation is given below [16]:

$$\begin{aligned} T_{\mathrm{em}} + T_{\mathrm{cogg}} + T_{\mathrm{reluct}} &= p \times [\phi]^t \times [i] \\ &= J \cdot \frac{\mathrm{d}\Omega}{\mathrm{d}t} + f \times \Omega + T_{\mathrm{load}} \end{aligned} \tag{2}$$

where T_{em}, T_{cogg}, T_{reluct}, and T_{load} are the electromagnetic, cogging, reluctance torques, and mechanical load torque, respectively. p is the number of pole pairs, $[\Phi]$ are the phase flux linkages, Ω is the rotor speed, J is the moment of inertia and f is the friction coefficient.

The objective of the control strategy is to maintain the same speed and also the same average torque after the fault was introduced. The maximum torque per ampere (MTPA) control is used and the simplified schematic of the model is depicted in Fig. 2.

This model is able to consider both the healthy and the faulty conditions. The faulty condition assumes that a single coil out of four is short circuited (fault severity is 25%) and that the adjacent PM works at a higher temperature due to the inter-turn short circuit, as in Fig. 3. The cases with different numbers of turns short-circuited can also be investigated using similar approaches.

For simplicity, the rest of the PMs are assumed to work at 25°C. This assumption might be arguable and to be more accurate, the thermal modelling of the entire machine before and after the short circuit is needed. However, this is out of the scope of this paper and will be carried out in future works.

Third, the finite element models are used again to assess the PM irreversible demagnetisation. They rely on output from the previous Matlab/Simulink models, namely the rotor position and current waveform variations in time. In order to accurately account for the demagnetisation, a special PM material model, as shown in Fig. 4, is used. This can recalculate the local map of remanent flux density within the affected PM if the local flux density drops below the knee point, which also means that the magnet is irreversibly demagnetised. The PM operation point, w, is compared with the knee point magnetic field H_k at each time step. If the local magnetic field has dropped below the knee point value, say the point d, the new PM operation point w' is established along a recoil line given by point d and B'_r. In this manner, performance degradation due to demagnetisation can be considered.

3 Inter-turn short-circuit current comparison

In Fig. 5, a comparison between the current waveforms for both the healthy and faulty conditions is shown for low and high temperatures (25 and 150°C, only for the affected PM, and other PMs are working at the operating temperature of 25°C). The machines operate under healthy conditions then the aforementioned short-circuit fault is introduced at around 0.2 s. The reference speed is 1000 rpm and the reference torque is imposed to rated values given in Table 1, which ensures all the machines operate at the same rated current before short circuit occurs. The 1000 rpm value is chosen in order to ensure that the fault effects due to short circuit can be observed during the investigations. At this value, the short-circuit current will be quite high, generating both important copper losses and demagnetising magnetic field.

As it was expected, the low temperature case yields the highest short-circuit currents for all the investigated machines. This is because the phase resistance in the affected coil increases with temperature rise, while the back-EMF decreases. The highest short-circuit current is reached by the SFPMM. However, when it comes

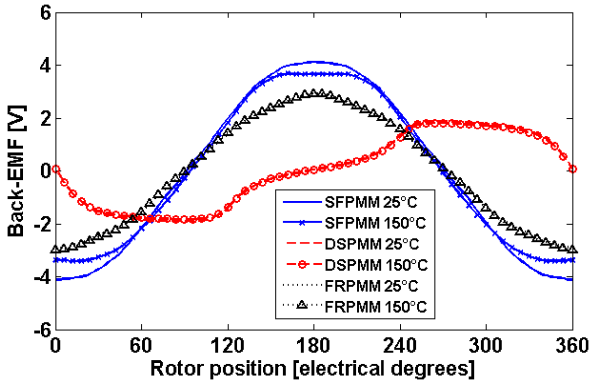

Fig. 6 *Phase back-EMF comparison for all topologies at low (25°C) and high (150°C) temperatures*

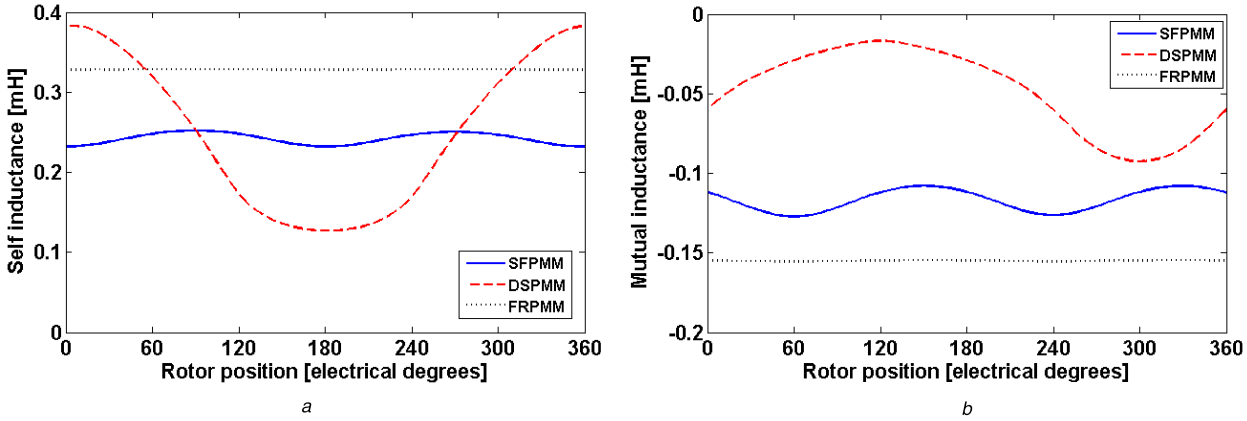

a *b*

Fig. 7 *Inductance variations with rotor position for all topologies*
(a) self-inductances, ***(b)*** mutual inductances

Table 2 Average self and mutual inductances for all topologies

	SFPMM	DSPMM	FRPMM
self, mH	0.242	0.249	0.329
mutual, mH	−0.117	−0.048	−0.155

to temperature effects on the short-circuit current value, it can be noticed for the DSPMM and the FRPMM that increasing the temperature barely affects their short-circuit currents. This can be explained by using (3), which is an analytical approximation of the short-circuit current i_{sc}:

$$i_{sc} \simeq \frac{\alpha \times E_{\max}}{\sqrt{(\alpha \times R)^2 + (\alpha^2 \times \omega \times L)^2}} \tag{3}$$

where α is the ratio of the short-circuited turns over the total phase turn number, R and L are the phase resistance and self-inductance, $E_{\max}$ is the magnitude of the phase back-EMF, while ω is the angular electric frequency. The short-circuit current is directly proportional to the back-EMF, which would explain the differences between the SFPMM, DSPMM and FRPMM, as shown in Fig. 6. Furthermore, when considering the phase self-inductance variation with rotor position, it can be noticed that the highest value is reached by the FRPMM which together with the back-EMF result would explain why FRPMM topology is subjected to the smallest short-circuit current.

The self- and mutual inductance variations with rotor position for all topologies are given in Fig. 7. It is noted that the self- and mutual inductances of the FRPMM topology are almost constant. This is due to the shape of the stator teeth and the large effective air-gap length. The average values for inductance are summarised in Table 2. The FRPMM has the highest self-inductance, which is useful in limiting the short-circuit current.

Based on the mutual inductance results, one can conclude that the DSPMM topology has the strongest magnetic separation between the phases, while the FRPMM is the worst. However, since all topologies considered are double layer, there is no thermal or physical separation at all between adjacent coils. To address this issue, the single-layer winding structure could be employed.

4 PM irreversible demagnetisation at high speed

The PM irreversible demagnetisation is studied under the aforementioned fault conditions for three temperatures: 25, 100, and 150°C, and all are at high speed (1000 rpm). The flux densities within the affected PM are studied next and compared with the knee point values (−0.08, 0.28, and 0.5 T for the three considered temperatures, respectively). At 25°C, all topologies are safe from demagnetisation, therefore, the results are not shown here. However, for higher temperature (150°C), almost the whole affect magnet will be demagnetised regardless of the machine topologies and this will be investigated first.

The flux density colour maps within the affected magnet under faulty conditions and at 150°C are given in Fig. 8. It is worth mentioning that the simulations with PMs as the only magnetic source were also carried out. This can be achieved by removing the armature field (produced by both the healthy and faulty coils) using the frozen permeability method [17]. The purpose of such simulations is to investigate the influence of the magnetic circuit on the PM working point at relatively higher temperature. Based on obtained results under fault conditions, it was found that for all topologies, there is very little difference in flux density with or without armature field. Therefore, one can conclude that the short-circuit current only contributes to increase the local temperature of the affected magnet but the demagnetisation process occurs mainly due to the influence of the rest of the magnetic circuit.

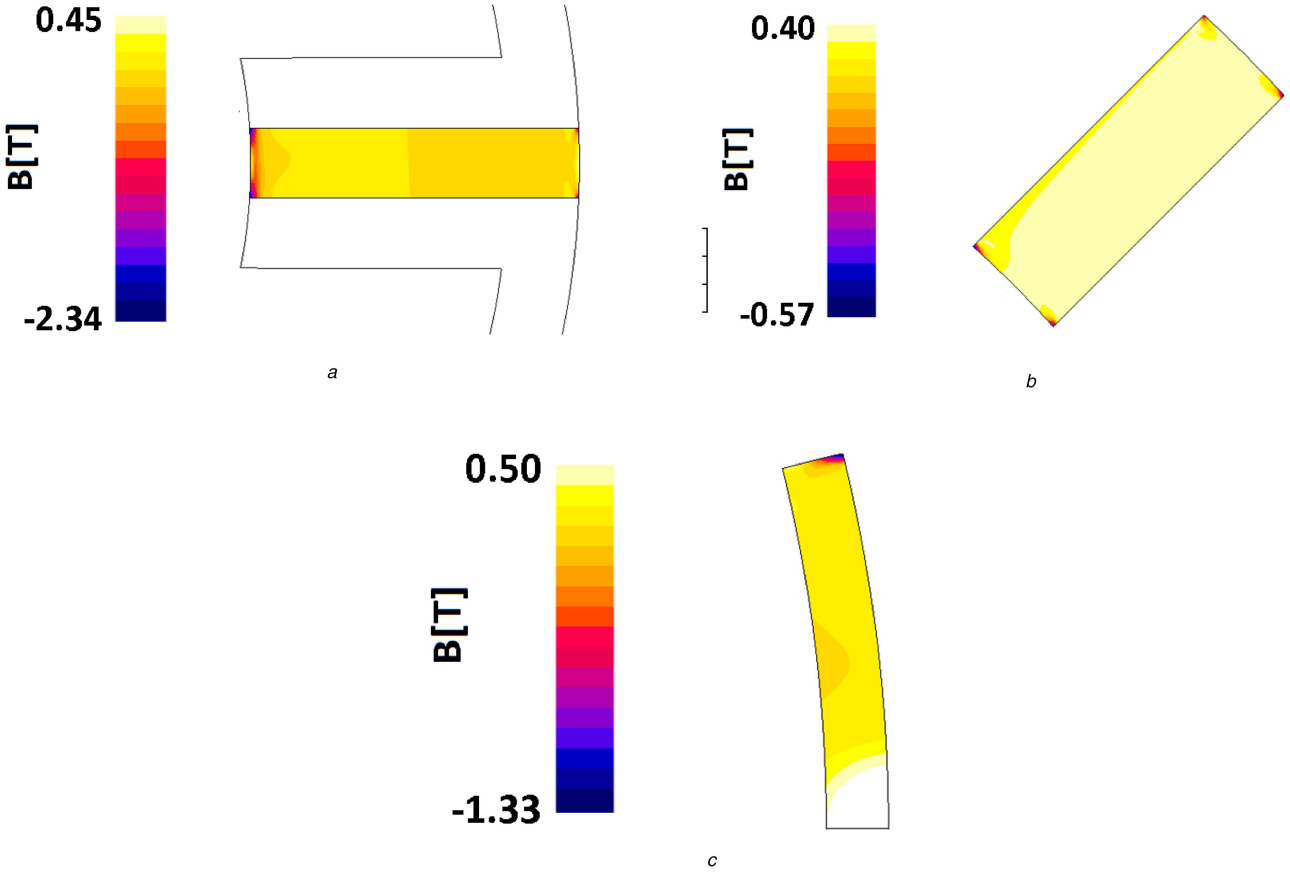

Fig. 8 *Flux density colour maps for all topologies at 150°C. Any coloured regions (< 0.5 T) value indicate irreversible demagnetisation*
(a) SFPMM, ***(b)*** DSPMM, ***(c)*** FRPMM

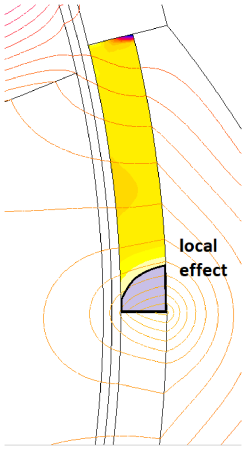

Fig. 9 *Flux lines showcasing local phenomenon for FRPMM*

The maps in Fig. 8 show that all topologies will experience severe irreversible demagnetisation at higher temperature. However, the PM of the FRPMM has a small area in which the flux density does not drop below the knee point value. When investigated further, as shown in Fig. 9, it was found that this is because of a local phenomenon caused by the close vicinity of the opposite sign PM. The neighbouring PM will enhance the local magnetic field thus ensure that the flux density is well above the knee point value, avoiding irreversible demagnetisation.

The results concerning the 100°C case are also given, as shown in Fig. 10. It can be seen that the most affected topology is the SFPMM, which gets completely demagnetised, followed by the FRPMM which is only partially affected. The DSPMM topology, however, does not demagnetise, thus being the most reliable when it comes to demagnetisation withstand capabilities.

The SFPMM demagnetisation process for 100°C case was detailed in [12] so only the FRPMM is investigated further here. The current sources are removed and only the PMs are kept in the model as the magnetic field source using the previously mentioned frozen permeability method. The results are shown in Fig. 11, and it can be seen that the demagnetisation process is mainly due to the magnetic circuit lowering the operation point of the PM on the B(H) curve and not due to the demagnetising magnetic field produced by the short-circuit current.

5 Conclusions

Three stator-mounted PM machines, namely the SFPMM, DSPMM, and FRPMM topologies, have been investigated from the point of view of fault tolerance to inter-turn short-circuit and irreversible demagnetisation. Their properties are summarised in Table 3. Due to their different magnetic circuit configurations, the DSPMM and FRPMM present large self-inductance and smaller back-EMF, which allow them to restrain the short-circuit current to reasonable values, closer to the rated one. The DSPMM is the most resilient to demagnetisation. Combining its excellent cost/

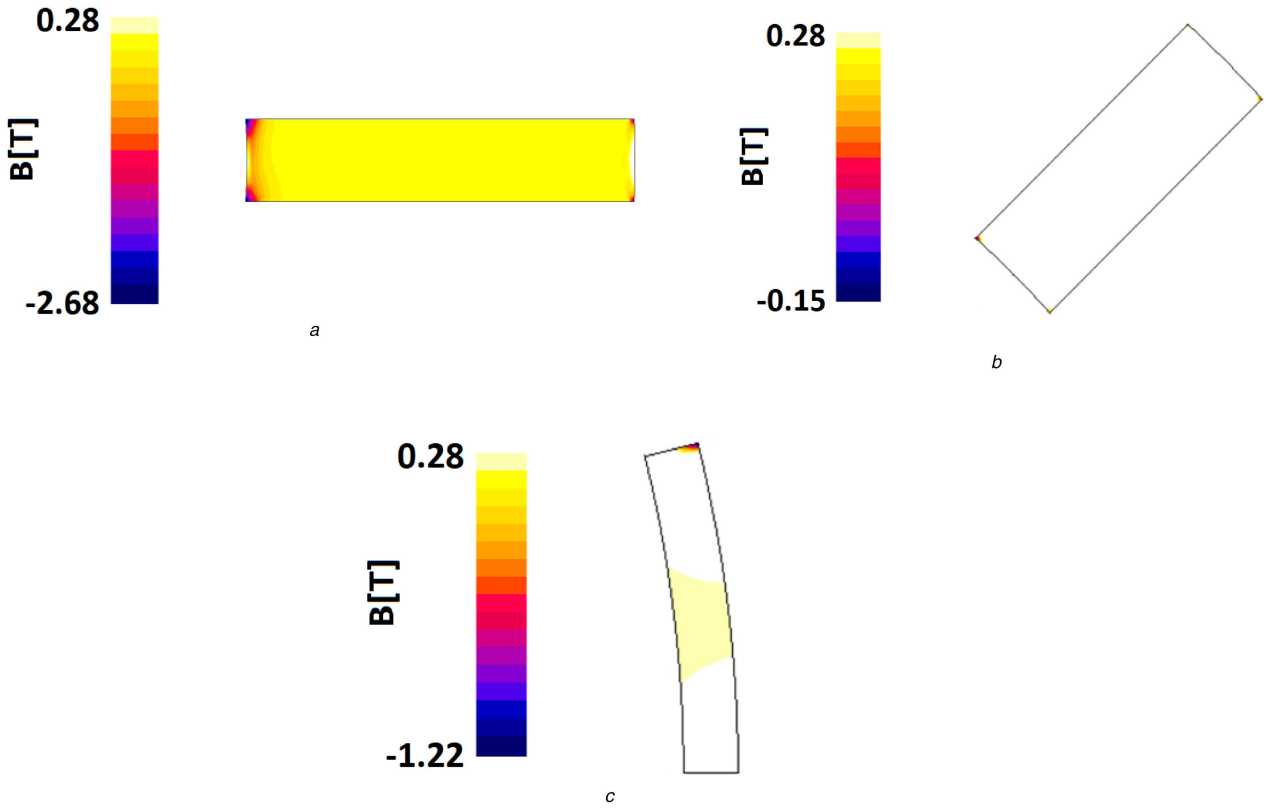

Fig. 10 *Flux density colour maps for all topologies at 100°C. Any coloured regions (< 0.28 T) indicate irreversible demagnetisation*
(a) SFPMM, ***(b)*** DSPMM, ***(c)*** FRPMM

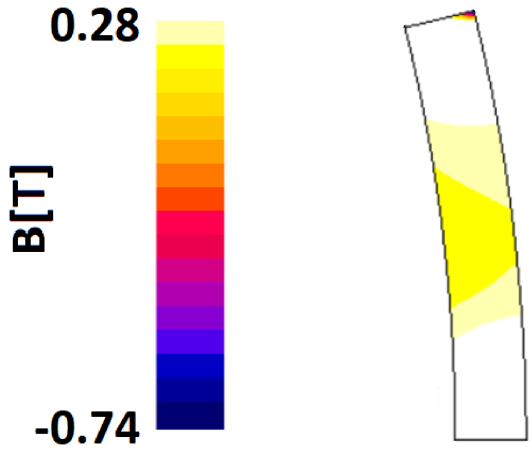

Fig. 11 *Flux density colour maps at 100°C for FRPMM without considering armature field. Any coloured regions (<0.28 T) indicate irreversible demagnetisation*

Table 3 Summary of investigated machines (SFPMM/DSPMM/FRPMM)

	SFPMM	DSPMM	FRPMM
torque/PM, mN/mm^3	0.12	0.267	0.275
peak short- circuit current [A] at 1000 rpm	46.1	28.1	27.8
demagnetisation withstand capability	poor	good	poor

performance makes it an interesting candidate for cost-effective applications. The FRPMM shows good capabilities in limiting the short-circuit current. Despite this, it was discovered that the demagnetisation process can still happen due to temperature effect alone. It is possible that increasing the thickness of the PMs for FRPMM will improve the demagnetisation withstand capability at the expense of overall performance. This will be investigated in future works.

6 References

[1] Hoang, E., Lecrivain, M., Gabsi, M.: 'A new structure of a switching flux synchronous polyphased machine with hybrid excitation'. 2007 European Conf. on Power Electronics and Applications, Aalborg, Denmark, 2007
[2] Liao, F., Liang, F., Lipo, T.A.: 'A novel permanent magnet machine with doubly saliency structure', *IEEE Trans. Ind. Appl.*, 1995, **3**, pp. 1069–1078
[3] Deodhar, R.P., Andersson, S., Boldea, I., *et al.*: 'The flux-reversal machine: a new brushless doubly-salient permanent-magnet machine', *IEEE Trans. Ind. Appl.*, 1997, **33**, pp. 925–934
[4] Cheng, M., Hua, W., Zhang, J., *et al.*: 'Overview of stator-permanent magnet brushless machines', *IEEE Trans. Ind. Electron.*, 2011, **58**, pp. 5087–5101

[5] Hua, W., Cheng, M., Zhu, Z.Q., *et al.*: 'Comparison of electromagnetic performance of brushless machines having magnets in stator and rotor', *J. Appl. Phys.*, 2008, **103**, p. 07F124
[6] Hua, W., Zhu, Z.Q., Cheng, M., *et al.*: 'Comparison of flux-switching and doubly-salient permanent magnet brushless machines'. Proc. Int. Conf. on Electrical Machines and Systems, Nanjing, China, 2005
[7] Fasolo, A., Alberti, L., Bianchi, N.: 'Performance comparison between switching-flux and IPM machine with rare earth and ferrite PMs'. Proc. Int. Conf. on Electrical Machines, Marseille, France, 2012
[8] McFarland, J.D., Jahns, T.M., El-Refaie, A.M.: 'Demagnetization performance characteristics of flux switching permanent magnet machines'. Proc. Int. Conf. on Electrical Machines 2014, Berlin, Germany, 2014
[9] Li, S., Li, Y., Sarlioglu, B.: 'Partial irreversible demagnetization assessment of flux switching permanent magnet machines'. Proc. Int. Conf. on Electrical Machines 2014, Berlin, Germany, 2014
[10] Afinowi, A.A., Zhu, Z.Q., Guan, Y., *et al.*: 'Performance analysis of switched-flux machines with hybrid NdFeB and ferrite magnets'. Proc. of Int. Conf. on Electrical Machines and Systems 2014, Hangzhou, 2014
[11] 'Arnold Magnetic Technologies'. Available at http://www.arnoldmagnetics.com, Accessed 2017
[12] Taras, P., Li, G.J., Zhu, Z.Q.: 'Comparative study of fault-tolerant switched-flux permanent-magnet machines', *IEEE Trans. Ind. Electron.*, 2017, **64**, pp. 1939–1948
[13] Li, G., Taras, P., Zhu, Z.Q., *et al.*: 'Investigation of irreversible demagnetization in switched flux permanent magnet machines under short-circuit conditions', *IET Electr. Power Appl.*, 2017, **11**, pp. 595–602
[14] Vaseghi, B., Nahid-Mobarakh, B., Takorabet, N., *et al.*: 'Inductance identification and study of PM motor with winding turn short circuit fault', *IEEE Trans. Magn.*, 2011, **47**, pp. 978–981
[15] Li, G.J.: 'Contribution à la conception des machines electriques à rotor passif pour des applications critiques: modélisations electromagnétiques et thermiques sur cycle de fonctionnement, etude du fonctionnement en mode dégradé'. PhD Thesis, 2011
[16] Ben Sedrine, E., Ojeda, J., Gabsi, M.: 'Fault-tolerant control using the GA optimization considering the reluctance torque of a five-phase flux switching machine', *IEEE Trans. Energy Convers.*, 2015, **30**, pp. 927–938
[17] Chu, W.Q., Zhu, Z.Q.: 'Average torque separation in permanent magnet synchronous machines using frozen permeability', *IEEE Trans. Magn.*, 2013, **49**, pp. 1202–1210